Hindawi
International Journal of Polymer Science
Volume 2018, Article ID 1090753, 20 pages
https://doi.org/10.1155/2018/1090753

Research Article

Effect of Variation of Hard Segment Content and Graphene-Based Nanofiller Concentration on Morphological, Thermal, and Mechanical Properties of Polyurethane Nanocomposites

Michał Strankowski

Chemical Faculty, Polymer Technology Department, Gdansk University of Technology, Narutowicza 11/12, 80-233 Gdansk, Poland

Correspondence should be addressed to Michał Strankowski; micstran@pg.gda.pl

Received 2 March 2018; Revised 4 July 2018; Accepted 28 July 2018; Published 6 September 2018

Academic Editor: Jeefferie Abd Razak

This study describes the development of a new class of high-performance polyurethane elastomer nanocomposites containing reduced graphene oxide (RGO) or graphene nanoplatelets (GNP). Two types of polyurethane elastomers with different contents of hard segments (HS) were used as a polymer matrix. The developed nanocomposites were characterized by thermal analysis (DSC, TG), dynamic mechanical testing (DMA), hardness testing, mechanical properties, rheology, FTIR spectroscopy, XRD, and microscopy investigation (TEM, SEM). Morphological investigation confirmed better compatibility of RGO with the polyurethane (PU) matrix compared to GNP. Both applied nanofillers influenced melting and crystallization of the PU matrix. The nonlinear viscoelastic behavior of the nanocomposites (Payne effect) was studied, and the results were compared with theoretical predictions.

1. Introduction

Many nanofillers are at present popular additives used to modify diverse properties of polymeric materials influencing their mechanical, physical, and chemical properties and durability parameters as well [1–3]. Nanofillers are often distinguished by the shape as nanoplatelets (1D), nanofibres (2D), or nanoparticles (3D) [3]. All of them should have at least one dimension down to 100 nm. Most commonly used nanofillers are silicates (includes the most popular montmorillonite), titanium dioxides, metallic nanoparticles, inorganic nanotubes, and all of the carbon nanofillers like carbon nanotubes, fullerenes, and finally graphene. When Geim and Novoselow in 2004 made a breakthrough in science with the discovery of graphene monolayers, the scientific community all over the world started focusing on these material properties and possible applications. Since then, improving methods of graphene synthesis and synthesis of different types of its derivatives were elaborated. Every single one of graphenes' derivatives, like graphene oxide (GO), chemically reduced graphene oxide (RGO), thermally reduced graphene (TRG), and chemically modified graphene (CMG), have different properties compared to pure graphene sheet. Every method of synthesis (from epitaxial methods, CVD, intercalation of graphite, exfoliation, etc.) provides a new material with specific characteristics.

Many polymers were already used to obtain graphene-based polymer nanocomposites. Most commonly used polymer matrices are polyethylene [4–6], polyamide 6 [7–9], poly(methyl methacrylate) [10–12], polystyrene [13–15], natural rubber [16–19], and polyurethanes [20–23]. Most of polymer nanocomposites showed better (comparing with nonmodified matrices) durability [24, 25] and good thermal properties [24] and gained some additional properties like electrical conductivity [25] and hydrophobic behavior [26]. Literature data reveal that using different types and contents of graphene-based nanofillers might improve a wide range of properties of polymers, especially polyurethanes [27–30].

Polyurethane elastomers are one of the most important polymeric materials, which can be applied in those areas, where use of classical elastomers is limited. Generally,

polyurethane elastomer macromolecular chains are built up of soft (SS) and hard (HS) segments [31], and the proportion of hard to soft segments and the polarity of the segments determine especially elasticity, hardness [32, 33], mechanical [33, 34] or thermal [33, 34] properties, and the morphology of PU. Intra- and intermolecular hydrogen bonds within polyurethane materials influence additionally the strength and thermal stability of these elastomers [35]. The low miscibility between soft and hard segments leads to microphase separation of segmented polyurethanes. Increasing HS content above 30% often evidently changes long-range connectivity of HS, and this results in an increase in mechanical strength of polyurethanes. What is more, chemical components like isocyanates, polyols, and chain extenders (it is symmetric and presents reactive groups), used to obtain polyurethane materials, may introduce specific interactions between the segments, which determine the thermal and mechanical behavior [35]. Properties of polyurethane elastomers can be also modified during processing by creating polymer nanocomposites [21, 36, 37], where the polyurethane material acts as a matrix for dispersed nanoparticles.

The present paper is aimed at reporting the influence of two carbon nanofillers (reduced graphene oxide (RGO) and graphene nanoplatelets (GNP)) on two polyurethane elastomeric matrices (possessing different hard segment (HS) contents). This also focuses on nanocomposite systems while gaining changes in some properties, such as improved mechanical and thermal properties. The morphology and viscoelastic behavior with changing stiffness of the matrix was also studied. Nanofillers used in this work were thermally reduced graphene (RGO) and graphene nanoplatelets (GNP). This is a new approach to obtaining nanomaterials based on the wide use of polyurethane raw materials, which should be suitable for a commercial application. The main goal was to obtain high-performance nanocomposites by simple methods of synthesis, such as in situ polymerization method, without solvents. Also, some of the synthesized nanocomposites contained nanofiller RGO derived from graphite. Compared to GNP, provided by the commercial manufacturer, but still expensive [38], usage of low-cost laboratory-made RGO is an economical approach to estimating the way towards mass scale production of graphene derivative-based nanocomposites.

RGO is an economical approach to estimating the way towards mass scale production of graphene derivative-based nanocomposites. Incorporation of these types of nanofillers can extend polyurethane thermoplastic elastomers' property limits, improving the mechanical and tribological performance of common TPU applications like footwear, closure o-rings and seals, adhesives, automotive interiors, and sport and leisure items. There here is a high-potential, still needed investigation for using GNP or RGO containing polyurethane nanocomposites in these technical goods, where electrostatic dissipation ability is of special importance, like conveyer belts and technical fabrics [38–40].

It is the first performed detailed study of the influence of the used nanofillers on hard and soft segment phase formation and property changes in polyurethane elastomer nanocomposites.

2. Methods and Materials

2.1. Differential Scanning Calorimetry (DSC). Differential scanning calorimetry measurements have been carried out by a heat-flux Netzsch DSC 209F1 Proteus analyzer. The calibration process was performed for 6 points ($C_{10}H_{16}$, In, Sn, Bi, Zn, CsCl). The investigation temperature range was from −85°C to 250°C. 5–10 mg samples were used in alumina pans. Measurement was performed in the N_2 atmosphere. During the investigation, a heating/cooling rate equal to 10°C/min was used. A second heating scan was used for the all calculations.

2.2. Thermogravimetric Analysis (TG). Thermogravimetry of obtained materials was conducted by a Netzsch TG 209F3 Tarsus analyzer. The calibration process was performed for 6 points (In, Sn, Bi, Zn, Al, and Ag). Investigations were performed using the Al_2O_3 crucible. Mass loss was followed at a heating rate of 20°C/min for samples (5–10 mg) in the temperature range from 37°C to 600°C, under N_2 atmosphere.

2.3. Dynamic Mechanical Analysis (DMA). Dynamical mechanical analysis has been carried out using a TA Instruments DMA Q800 analyzer. Investigation has been performed using tension mode, in the temperature range − 100–100°C, frequency equal to 1 Hz, and heating rate at 4°C/min. Samples were cooled using liquid nitrogen. Strain sweep analysis, for nonlinear viscoelastic investigation, has been conducted at temperature 35°C, in the same tension mode and frequency of deformation but in the amplitude range from 0.5 to 6500 μm.

2.4. Fourier Transformation Infrared Spectroscopy (FTIR). Fourier transformation infrared spectroscopy of polyurethane materials has been carried out using a Thermo Electron Corporation Nicolet 8700 Spectrometer (equipped with ATR mode). Samples were scanned from 4000 to 500 cm^{-1}.

2.5. X-Ray Diffraction (XRD). A Bragg-Brentano X'Pert Philips diffractometer was used to characterize prepared materials (40 kV, 30 mA, λ Cu Kα = 0.1542 nm). All samples were scanned from the 5 to 35° 2θ range.

2.6. Scanning Electron Microscopy (SEM). Scanning electron microscopy was performed using FEI Quanta 250 FEG (20 kV, LFD detector) with EDAX Apollo X-SDD EDS module.

2.7. Transmission Electron Microscopy (TEM). Microscopy analysis was performed using STEM-EDX Transmission Electron Microscope FEI Europe, Tecnai F20 X-TWIN coupled with EDX spectrometer. All samples were cut in cryo-mode using an ultramicrotome (Leica EM UC7 Ultramicrotome). HRTEM (for nanocomposite systems) was from JEOL, model JEM-2100. The thickness of the samples

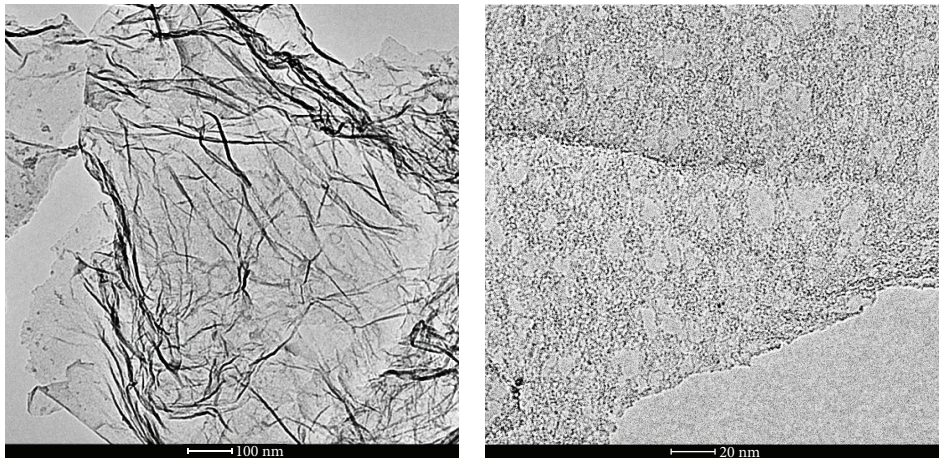

(a) (b)

Figure 1: TEM microphotographs of (a) thermally reduced graphene oxide (RGO) and (b) graphene nanoplatelets (GNP).

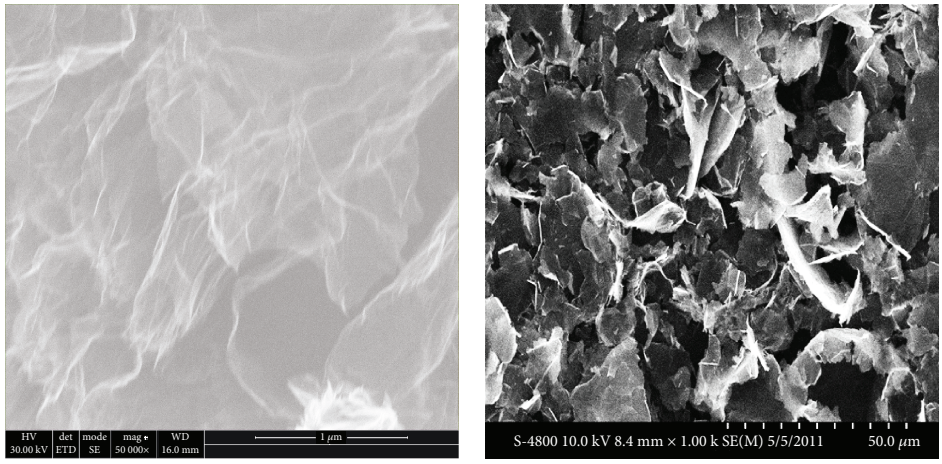

(a) (b)

Figure 2: SEM microphotographs of (a) thermally reduced graphene oxide (RGO) and (b) graphene nanoplatelets (GNP).

was 150 nm and was collected on a 200-mesh Cu grid before investigation.

2.8. Materials

2.8.1. Graphene Nanoplatelets. Graphene platelets (GNP) from ACS Materials (USA) [41] have 2–10 nm height (with 4–20 layers) and 20–40 m^2/g surface area (Figures 1(b) and 2(b)).

2.8.2. Reduced Graphene Oxide. Potassium permanganate ($KMnO_4$, >99%), hydrogen peroxide (H_2O_2, 30%), sulfuric acid (H_2SO_4, 35–38%), phosphoric acid (H_3PO_4, 85%), sulfuric acid (H_2SO_4, 96%), ethanol (C_2H_5OH, 96%), and diethyl ether ($(C_2H_5)_2O$,), all substrates from POCH SA., Poland, were used to obtain graphene oxide. Ar (>99% mol.) was used to perform thermal reduction of graphene oxide GO (Figures 1(a) and 2(a)).

2.8.3. Polyurethanes. The isocyanate used was 4,4′-methylene diphenyl diisocyanate (MDI), isocyanate content of 32 wt%, and an average functionality of 2.15, purchased from Zachem (Poland). The catalyst Dabco VR 33-LV-33 wt% solution of 1,4-diazobicyclo[2.2.2]octane in 2,2-dihydroxyisopropyl ether, short-chain hard-segment extender was 1,4-butanediol (1,4-BDO, from BASF, Germany), and polyol, poly(tetramethylene ether)glycol (PTMG, 1889 g/mol) was obtained from BASF, Hungary.

The method of the previous publication, Strankowski et al. [42], was followed.

3. Preparation

3.1. Reduced Graphene Oxide (RGO) Preparation. Two-step synthesis was used to obtain reduced graphene oxide (RGO). Based on modified Hummer's method, the GO nanofiller was prepared [43]. GO was thermally reduced to RGO at 200°C, using the Ar atmosphere.

3.2. Polyurethane (PU) Nanocomposite Preparation. Polyurethane materials were obtained using the two-step preparation

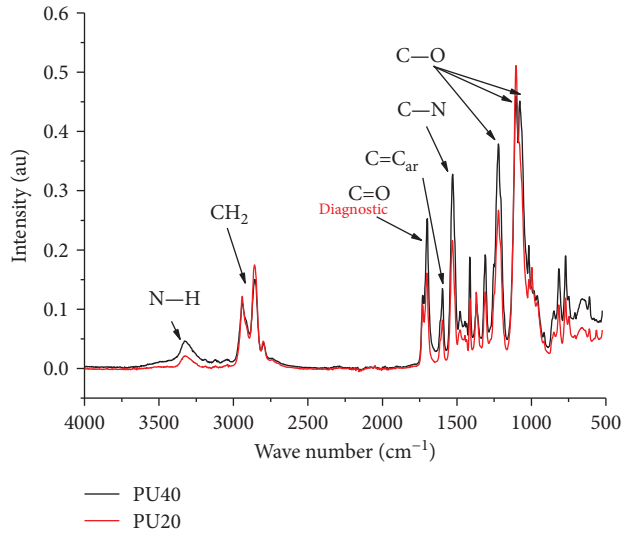

Figure 3: FTIR spectra for nonmodified PU with different hard segment ratios.

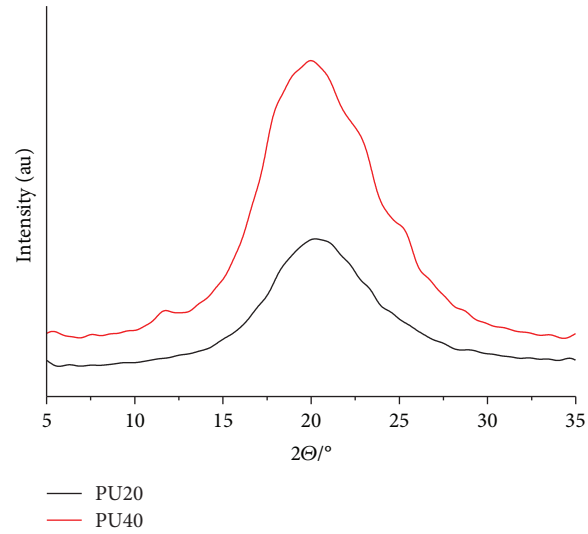

Figure 4: XRD diffractograms for nonmodified PU matrices with different hard segment ratios.

method with different hard segment (HS) contents of 20% (PU20) and 40% (PU40) by weight and at an isocyanate index equal to 1.05. The prepolymer was obtained at the first step by reacting PTMG polyol and MDI isocyanate at 70°C during 1 h under low pressure. The obtained prepolymer was used to prepare unmodified polyurethanes and nanocomposites. For unmodified systems at the second step, 1.2-butanediol (BD) as a chain extender and 1,4-diazabicyclo[2.2.2]octane (DABCO) as a catalyst were used. For preparing nanocomposite systems, a calculated amount of the nanofiller was mechanically (2500 rpm) dispersed in the prepolymer with ultrasound support for 30 min. At the last stage, to complete the reaction, BD and DABCO were added to the prepolymer containing the dispersed nanofiller. The reacting mixtures, when still fluid, were poured into the steel mold and annealed at 100°C for 24 h in a laboratory drier. After that, materials were compressed (2 tons) using a hydraulic press (Manual Hydraulic Press, Specac) to obtain thin 0.5 mm films, which were used for the investigations.

Samples designation: Notation PU20-1% GNP is the polyurethane matrix (PU) with proper amount hard segment content (20), containing 1 wt.% of the GNP nanofiller (1%GNP). Matrix|hard segment content|-|% weight of nanofiller|type of nanofiller|.

3.3. Unmodified Polyurethane Matrices (PU). Based on spectroscopy investigation, it was confirmed that general absorption bands are typical for the polyurethane matrices (Figure 3) [44, 45]. This study was performed to check that all reactions were completed and there were no visible bands for unreacted NCO groups from isocyanate substrates. What is more, X-ray diffraction analysis shows absence of diffraction maxima characteristic for crystalline regions (Figure 4) [46]. This study reveals that there are no long-range ordered structures in these polyurethane matrices. In Figure 4, a wide amorphous diffusion peak (at about $2\theta = 20^{\circ}$) can be observed which is typical for amorphous phase in amorphous and partially crystalline polymers [47–49].

Table 1: Phase transitions parameters for nonmodified PUs.

PU matrix	T_g (°C)	T_{mSS} (°C)	ΔH_{mSS} (J/g)	T_{mHS} (°C)	ΔH_{mHS} (J/g)	T_{cHS} (°C)	ΔH_{cHS} (J/g)
PU20	−41	25	13.5	212	5.5	111	−7.5
PU40	−46	25	12.0	190	9.1	119	−10.3

T_m: melting temperature; T_c: crystallization temperature; ΔH_m: enthalpy of melting; ΔH_c: enthalpy of crystallization.

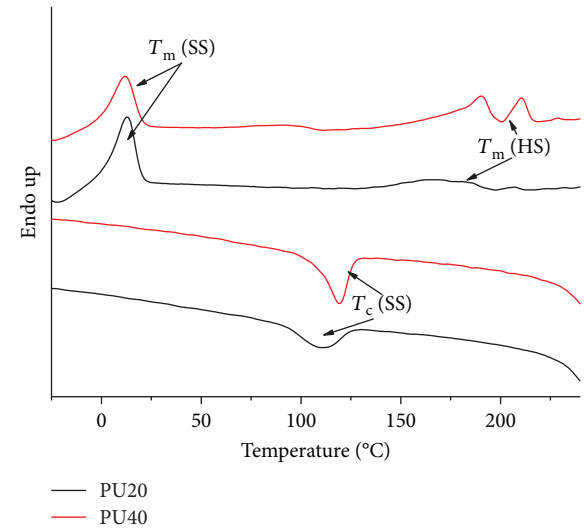

Figure 5: DSC thermograms for nonmodified PU matrices possess different hard segment contents.

For the polyurethane with higher hard segment content (PU40), higher temperature and enthalpy of melting point (T_m) were observed, in comparison to the softer matrix (PU20) (Table 1, Figure 5). The crystallization temperature for PU40 shifts to higher values (about 10°C) comparatively to the PU20 matrix, and enthalpy of crystallization has

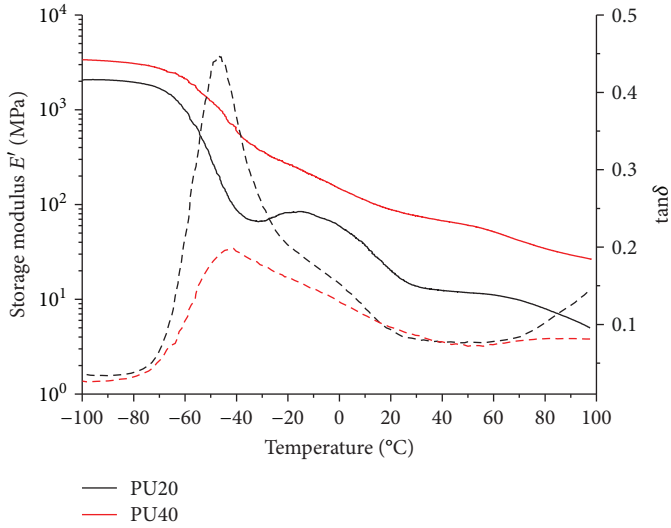

Figure 6: Storage modulus (E'/MPa—black line) and loss tangent (black dot line) versus temperature/°C for nonmodified PU matrices with different hard segment contents.

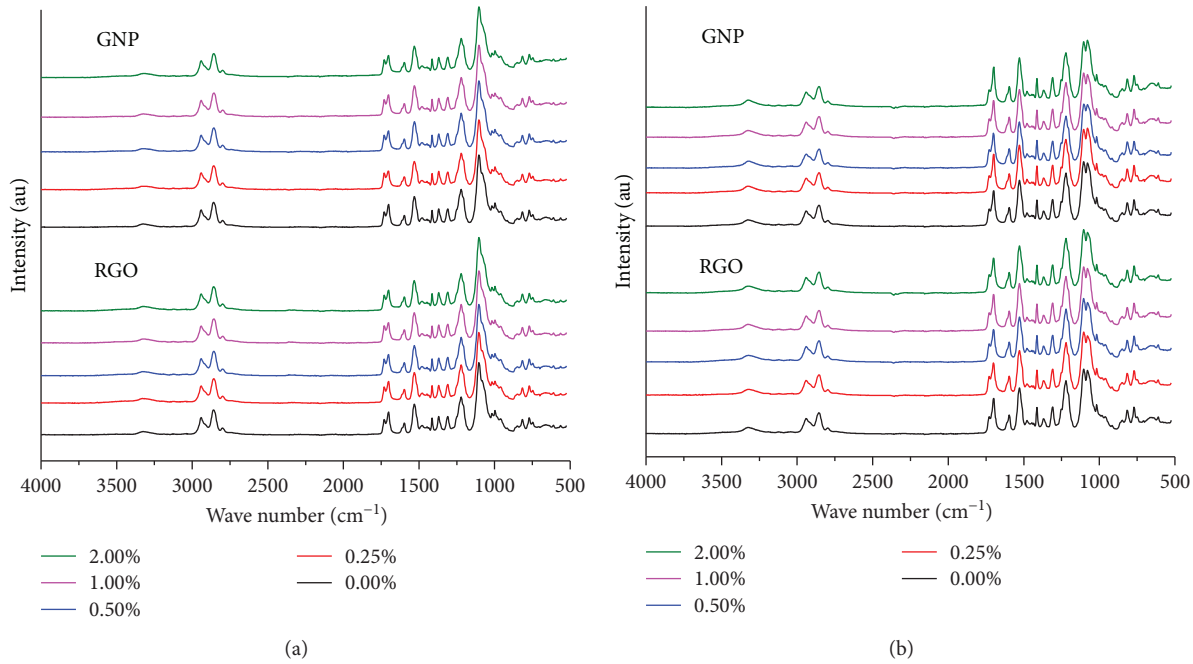

Figure 7: FTIR for (a) PU20 and (b) PU40 nanocomposites.

higher values for the harder matrix (PU40) (Figure 5). These results are in good agreement with the DMA study (Figure 6), where a higher storage modulus (E'/MPa) was observed for the PU40 matrix in the applied temperature range for this investigation.

4. Results

4.1. Polyurethane Nanocomposites

4.1.1. FTIR Spectroscopy. Infrared spectroscopy was performed for all nanocomposite materials containing RGO or GNP nanofiller. By comparing the FTIR spectra, it was confirmed that the addition of the nanofiller did not influence the chemical structure of the polyurethane matrix (Figure 7). However, there was a possible reaction of isocyanate groups with functional groups located on the surface of reduced graphene oxide. Nevertheless, the number of these reactive groups is negligible (max. 2%) and their influence of the nanocomposite creation is minor.

Based on the FTIR study where the absorption and diffraction of infrared radiation have low influence on waveforms (at such low content of the nanofiller) and, what is more, that the absorption coefficient of C=O and N–H bands

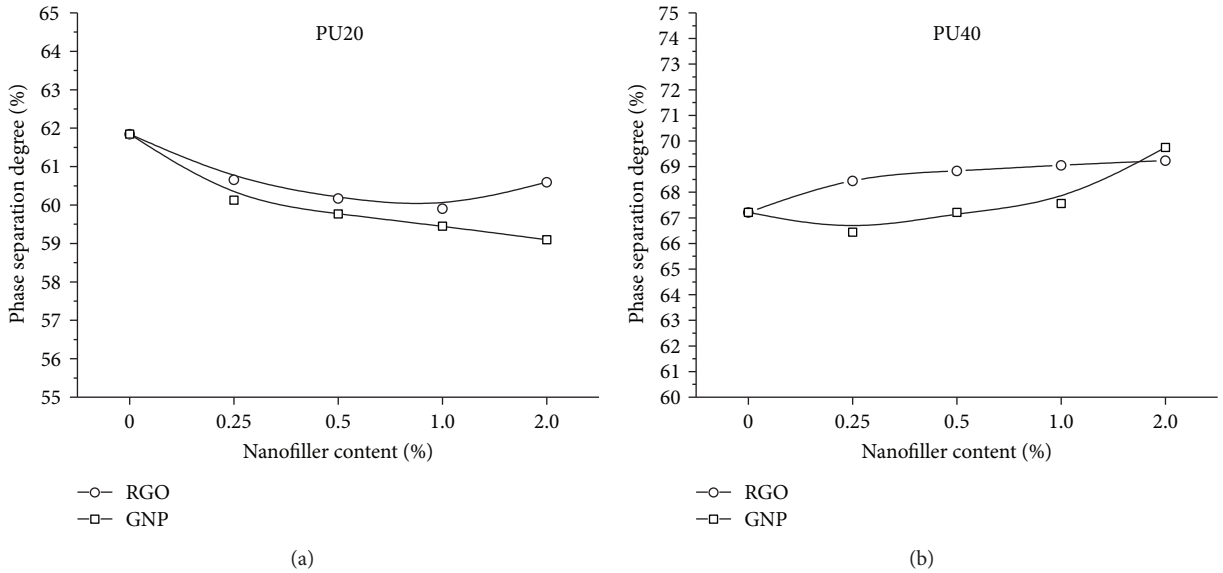

Figure 8: Phase separation degree (PSD) for (a) PU20 and (b) PU40 nanocomposites.

did not change, the phase separation behavior should be connected only with disorders of the domain structure caused by nanofiller addition. Phase separation was calculated according to [50–52] [for ~1730 cm^{-1} and ~1700 cm^{-1} bands; $PSD = R/(R+1)$, where $R = A_1/A_2 - NCO$ index, where A_1 and A_2 are surface areas of oscillating bands of the C=O group, hydrogen-bonded and nonhydrogen-bounded)], and the influence of nanofillers on this parameter is presented in Figure 8. It was confirmed that the phase separation degree (PSD) increased for PU40 nanocomposites and had lower values and decreased for PU20 materials (Figures 8(a) and 8(b)).

4.1.2. X-Ray Diffraction (XRD). The obtained diffractograms (Figure 9) for nanocomposites PU20-GNP and PU40-GNP show wide halo patterns originating from amorphous polyurethane materials. Moreover, for nanocomposites containing a GNP nanofiller, a diffraction maximum at about $2\theta = 27^\circ$ was visible, originating from crystalline layers of GNP. The intensity of these maxima increases with increasing content of the GNP nanofiller in the polyurethane matrix. For polyurethane nanocomposites, no diffraction maxima were observed, which confirmed (with TEM investigation support) that all the systems possess an exfoliated structure with a well-dispersed RGO nanofiller.

4.1.3. Transmission Electron Microscopy (TEM). Based on transmission electron microscopy (TEM) analysis, good dispersion of the nanofiller (RGO or GNP) into polyurethane matrices with different hard segment (HS) contents was confirmed. This is a very important factor characterizing the morphology of the nanofiller (size, dispersion) in nanocomposite systems. Reduced graphene oxide (RGO) and graphene nanoplatelets (GNP) (Figure 10) are visible in the form of characteristic long, disordered dark lines into clear, gray, PU matrices. For PU/GNP systems (Figures 10(a) and 10(d)), long lines (about 500 nm) are observed, which are aggregated into PU matrices (PU20 or PU40). For PU/GNP systems (Figures 10(a) and 10(d)), larger agglomerates were observed in comparison to the RGO-filled systems. The incorporation of RGO into the PU matrix causes good dispersion, and a characteristic disordered structure (short, thin, black lines) was obtained, as clearly observed in Figures 10(b), 10(c), 10(e), and 10(f). The RGO nanofiller is affected by the hard and soft segment ratio in the PU matrix, and better exfoliation is archived for the PU matrix with lower content of hard segments (Figures 10(b) and 10(c)). The RGO nanofiller has better compatibility to the polyurethane matrix (what relates to the –O– or –OH group on the surface of the nanofiller), and therefore higher dispersion is achieved.

These results based on TEM analysis are in good correspondence to the XRD study where (no diffraction maxima; described in X-ray diffraction (XRD) paragraph) an exfoliated nanocomposite morphology was confirmed, especially for PU/RGO materials.

4.1.4. Differential Scanning Calorimetry (DSC). Crystalline and amorphous domain structure changes in the obtained polyurethane nanocomposites were investigated using DSC. Figures 11 and 12 show DSC and cooling and heating scans. Based on cooling thermograms, it is visible that nanofiller addition (RGO and GNP) influences on polyurethane hard and soft domains. The temperatures of crystallization and enthalpies of this process change when the nanofiller is incorporated into the polyurethane matrix. For PU20-GNP and PU40-RGO, the nanofiller affects the rate of crystallization, where maximum temperature rates are lowest and enthalpy of crystallization takes the lowest values. This behavior is connected with a smaller amount of crystalline phase creation during cooling. However, samples PU20 (0.25 wt% GNP) and PU40 (2 wt% RGO) exhibit a shift in crystallization temperature of HS to higher temperatures, in comparison to the other modified materials. This behavior can be

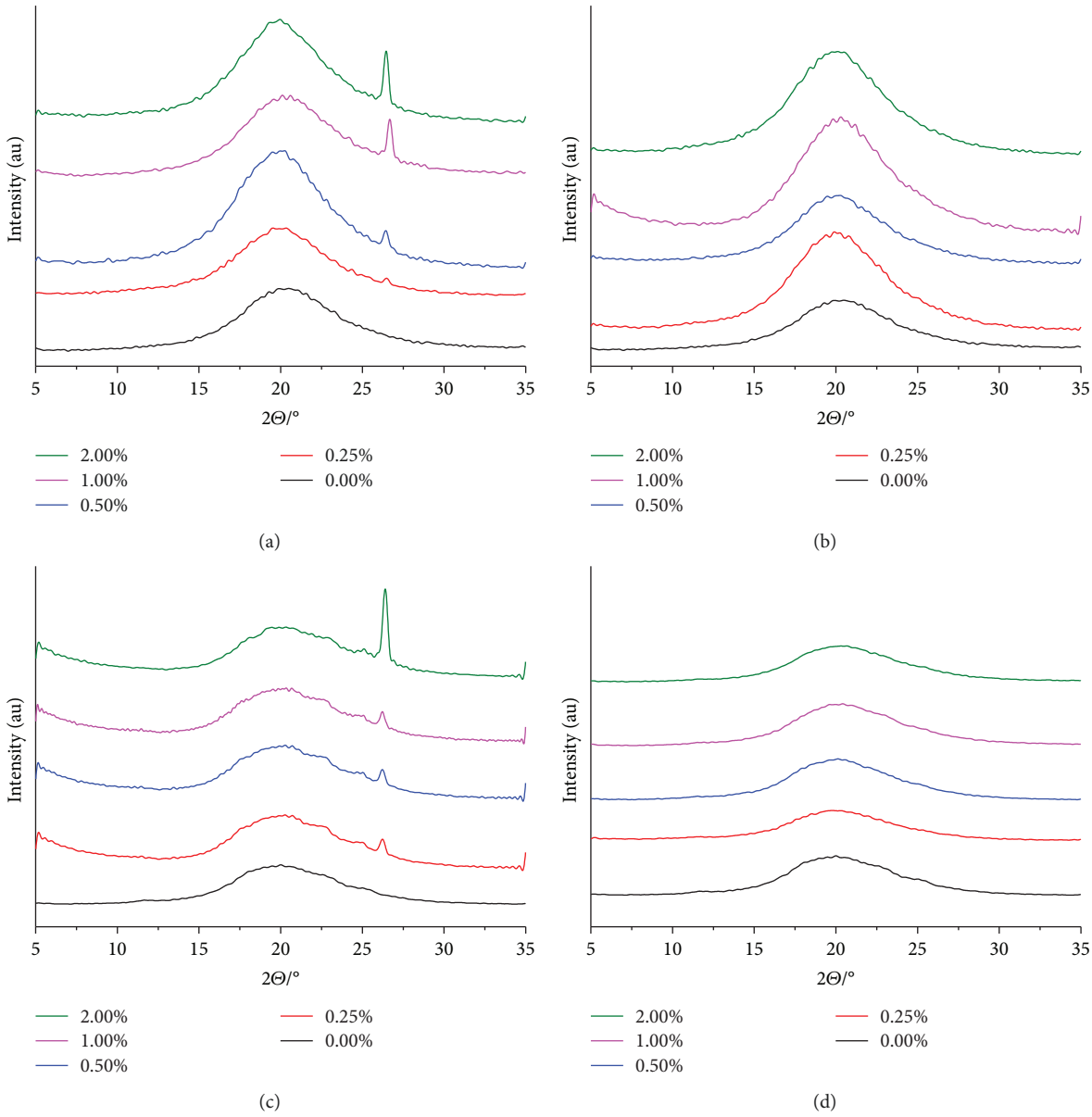

Figure 9: XRD for (a) PU20-GNP, (b) PU20-RGO, (c) PU40-GNP, and (d) PU40-RGO nanocomposites.

explained with possible presence of some impurities from the mold, which can infect the crystallization process of these materials. What is more, a reverse behavior exhibits PU20-RGO and PU40-GNP, where the crystallization temperatures are higher, which is related with the heterogenic nucleation process occurring at nanofiller surfaces. Additionally, for PU40-GNP nanocomposites, the observed crystallization peaks (shift to the higher temperatures) split with visible two maxima (Figure 11(c)), which is connected with creating crystalline areas of different size. Addition of the nanofiller also increases the crystallization rate of soft segments (SS), which is visible for all the PU40-GNP nanocomposites (Figure 11(c)), but not revealed for RGO-based nanocomposites, because this process could be extended in time after the controlled cooling step.

After the cooling process, all samples were heated at a controlled speed (second heating step, after clearing the thermal history of the samples) to verify the phase transition-melting behavior. For PU20-GNP, PU20-RGO, and PU40-RGO, the addition of the nanofiller causes a decrease in enthalpy of melting, which is connected with the lower amount of crystalline phase in the hard segment domains. Not very clear melting peaks for PU20 nanocomposites (at temperature range 125–210°C) were blurred in comparison to the nonmodified PU matrix. What is more, for PU40-RGO, there were revealed multiple peaks on the thermograms. The first maximum was visible at a temperature of about 90°C and the other two peaks at 190°C and 210°C (Figure 12(b)). The first maximum occurs before the melting point, and the next two maxima are connected with melting and recrystallization of the crystalline phase. The addition of the reduced graphene oxide (RGO) nanofiller, into the polyurethane matrix, causes an increase of the peak at 90°C, blurry peak at temperature 190°C, and extinction

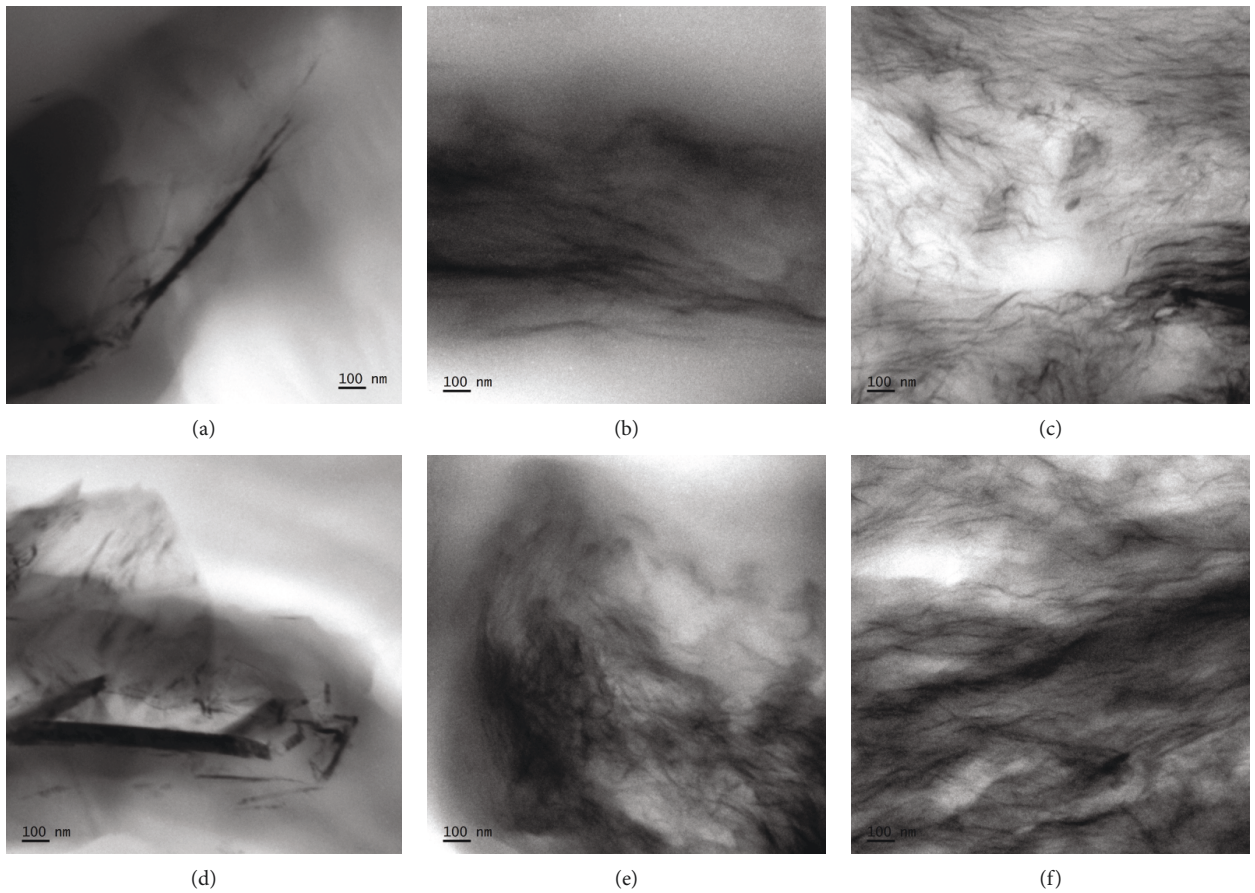

Figure 10: TEM microphotographs of (a) PU20/GNP1%, (b) PU20/RGO1%, (c) PU20/RGO2%, (d) PU40/GNP1%, (e) PU40/RGO1%, and (f) PU40/RGO2%.

of the maximum at 210°C (Figure 12(b)). Additionally, for the 2 wt% RGO nanocomposite, a wide region of melting at temperature 210–220°C is visible (Figure 12(b)). For PU40-GNP nanocomposites, enthalpy of melting shows no considerable difference in comparison to the PU40 matrix (Table 2). However, in the thermograms (Figure 12(b)), some configuration changes of melting peaks have been observed. At 190°C, the melting peak is lower and disappears with the addition of the 2 wt% GNP nanofiller. What is more, the second peak at 210°C is lower (up to 1 wt% GNP) and increases with the addition of 2 wt% in the nanofiller (GNP). Simultaneously for all nanocomposite systems, a third, well-defined, peak at 225°C is observed. For all heating runs, it is visible that the melting temperature of soft segment (SS) domains can be estimated at about 13°C (Figure 12(b)). Also, there was an observed decrease in the crystalline phase for nanocomposites PU20-GNP (above 0.5 wt% of the GNP nanofiller), PU40-RGO (for amount 0.25–1 wt% RGO), and PU20-RGO (for mount 0.5–1 wt% RGO), which is connected with lower values of melting enthalpy (Table 2). However, for PU40-GNP nanocomposites, this parameter (amount of crystalline phase within soft domains) remains at a similar level (Table 2).

4.1.5. Thermogravimetric Analysis (TG). Based on the performed TGA analysis, there was a confirmed slight improvement in the thermal stability of the nanocomposite system by the addition of the nanofiller (RGO or GNP). The onset degradation temperature of obtained materials is comparable for unmodified and nanocomposite systems (Figure 13, Table 3). For the modified system, this parameter shifts to higher temperatures at about $T_{5\%} = 5 - 7$°C in comparison to the polyurethanes without the nanofiller. Visible improvement in thermal stability (11°C) is observed for the PU40-RGO system with the 2 wt% nanofiller (Figure 13(f)). Maximum degradation temperatures (T_{DTGmax}) of hard segments (HS) for PU20-RGO (Figure 13(d)) and PU40-RGO (Figure 13(h)) are shifted to higher values by 27°C and 14°C, respectively (Table 3). For all nanocomposite systems, the degradation temperature of soft segments possesses similar values. For filled systems, there is a visible higher mass content [5% for PU20–2.0% GNP/RGO (Figures 13(a) and 13(b)) and 9% for PU40–2% GNP (Figure 13(e))] after degradation (mass residue), which is connected with higher thermal stability of nanofillers in comparison to the pure polyurethane matrices (2% for PU20 and 5% for PU40) (Figure 13, Table 3).

4.1.6. Dynamic Mechanical Analysis (DMA)

(1) DMA (Temperature Investigation). Thermomechanical parameters were collected in Figures 14 and 15, and the

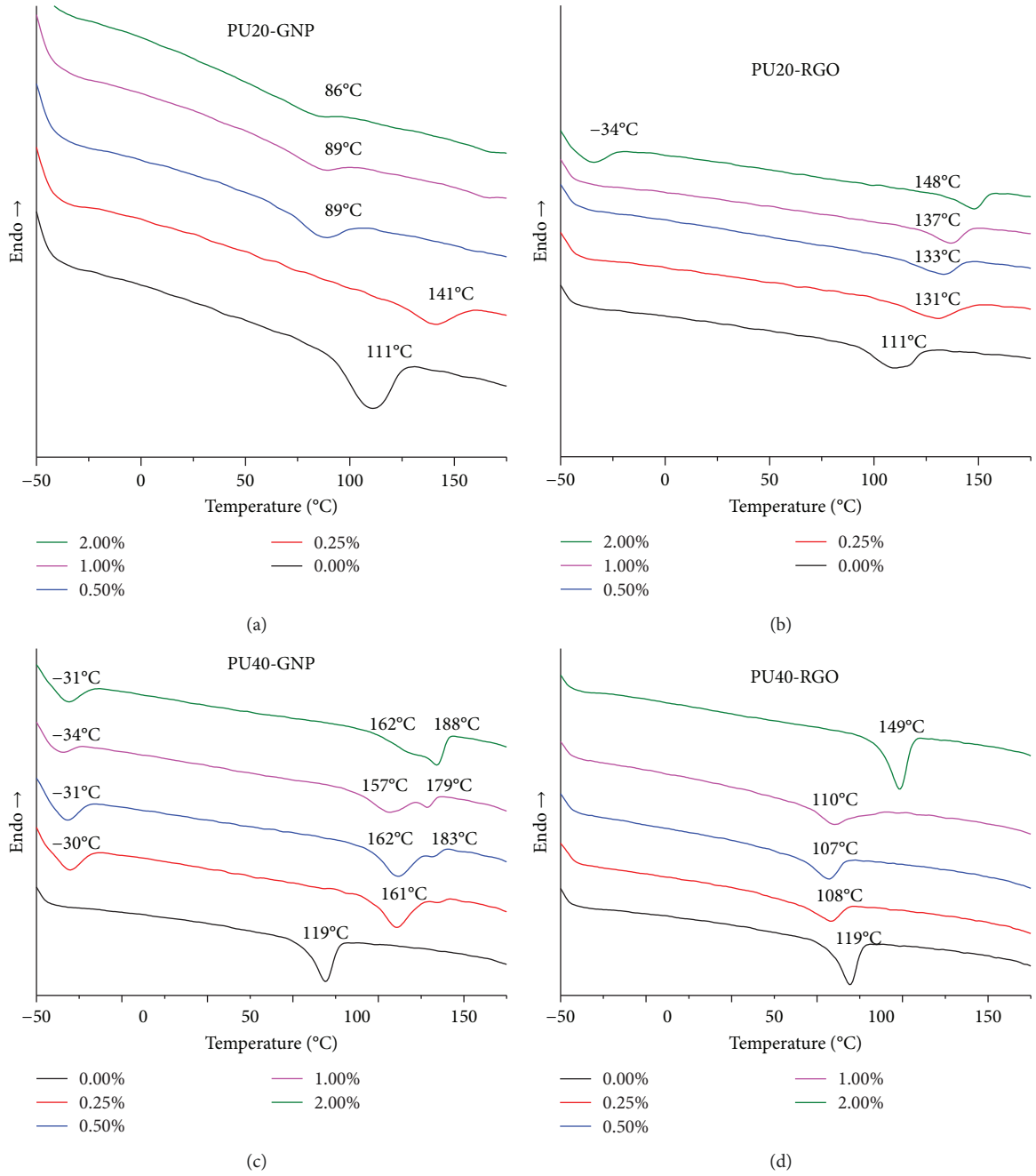

Figure 11: DSC thermograms for PU nanocomposites (cooling scans).

discussion of the results refers to specific regions which describe the polymer nanocomposite behavior (from glassy region to rubbery state, characteristic for polymeric materials).

(i) Glassy and viscoelastic area (temperature range: −100°C to −30°C)

Addition of the nanofiller does not cause significant changes in DMA characteristic parameters: storage modulus (E'), loss modulus (E''), and loss tangent (δ) in the glassy state temperature rage (Figures 14 and 15). Visible changes were observed above glass transition temperatures, where soft segments are at viscoelastic state and their movement is possible. It was confirmed that for polyurethane nanocomposites slightly lower values of the loss tangent were registered in comparison to the nonmodified PUs (Figures 14(e), 14(f) and 15(e), 15(f)). The glass transition temperature (calculated from the maximum of (tanδ)) changed with the addition of the nanofiller with a decrease of 6°C for PU20-2% RGO and an increase of about 4°C for PU20-2% GNP. For stiffer nanocomposite matrices with RGO and GNP nanofillers, a decrease in glass transition temperature in the range (1–9°C) was evident (Figures 14 and 15, Table 4). For PU40-0.5% GNP glass transition, the temperature shifts to the temperature of −51°C, with a value lower by 9°C compared to the nonmodified PU40 system (−42°C)

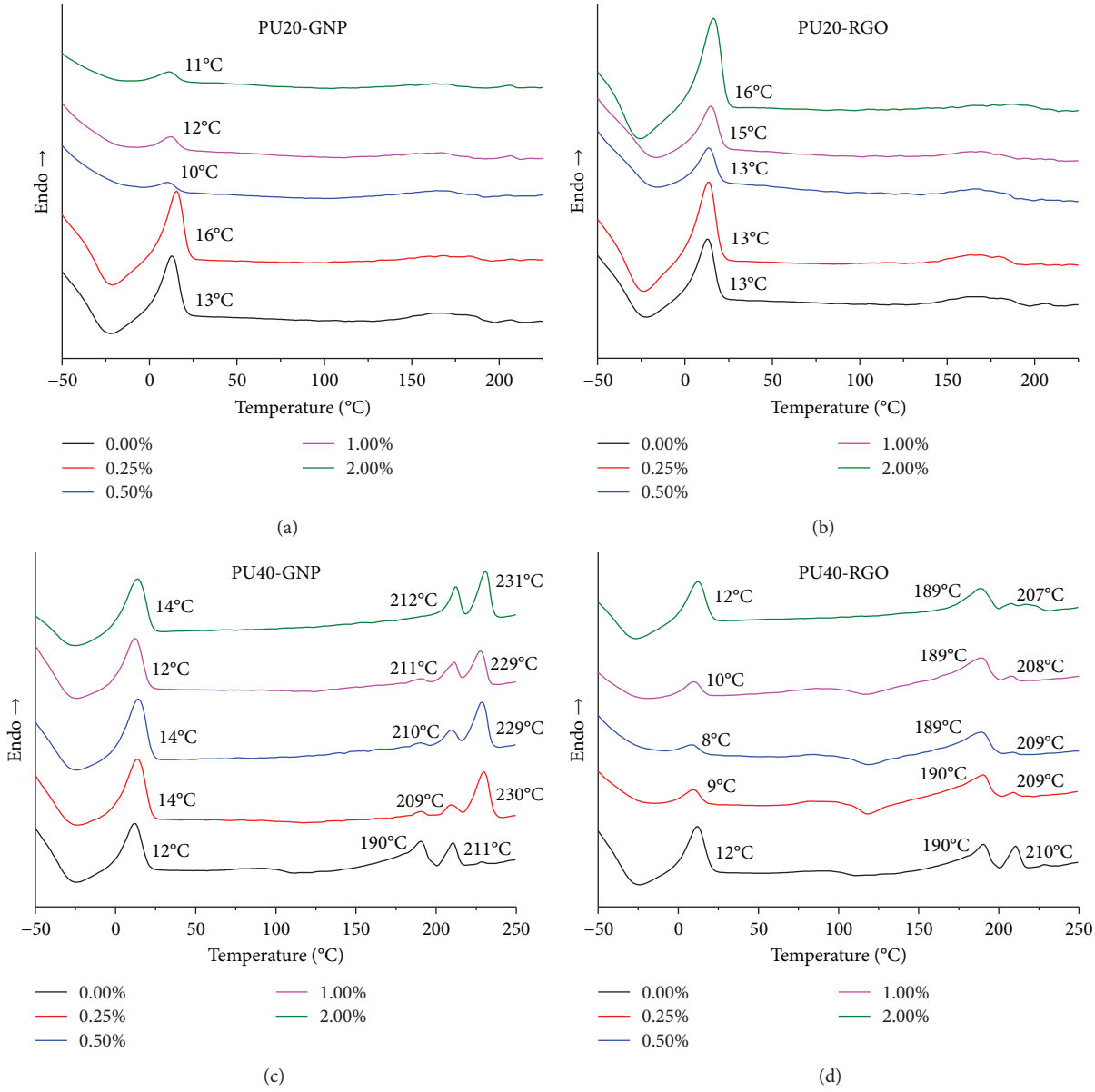

Figure 12: DSC thermograms for PU nanocomposites (heating scans).

Table 2: Enthalpy of melting for PU nanocomposites (heating scans).

% nanofiller	Heating scans							
	PU20-GNP		PU20-RGO		PU40-GNP		PU40-RGO	
	$\Delta H_{m,HD}$ (J/g)	$\Delta H_{m,SD}$ (J/g)	$\Delta H_{m,HD}$ (J/g)	$\Delta H_{m,SD}$ (J/g)	$\Delta H_{m,HD}$ (J/g)	$\Delta H_{m,SD}$ (J/g)	$\Delta H_{m,HD}$ (J/g)	$\Delta H_{m,SD}$ (J/g)
0.00	5.5	13.5	5.5	13.5	9.1	12.1	9.1	12.1
0.25	2.3	14.7	7.1	18.6	9.2	17.7	5.3	3.1
0.50	3.1	1.4	2.6	7.0	9.4	17.6	3.6	1.9
1.00	3.3	1.5	4.4	10.2	8.5	14.3	5.1	3.3
2.00	3.0	1.1	5.3	23.2	10.3	16.3	5.2	12.7

(Figure 14, Table 4). A higher decrease in glass transition temperature was observed for graphene nanoplatelet- (GNP-) based nanocomposites parallel to nanocomposites with reduced graphene oxide (RGO).

(ii) Soft domain melting area (temperature range: −30°C to 20°C)

At this specific range (−30°C to 20°C) within soft segment domains, crystalline forms are dispersed in the amorphous

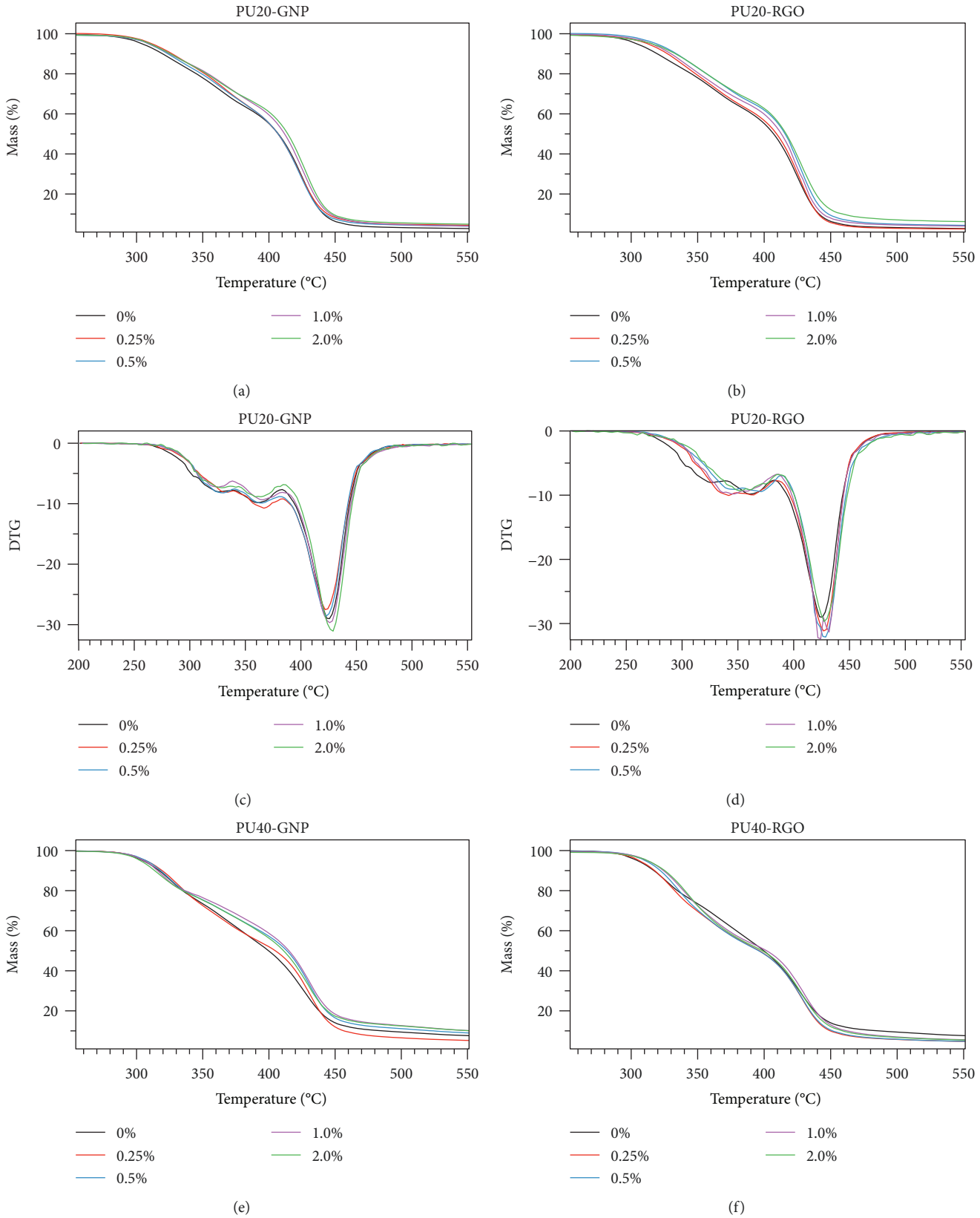

Figure 13: Continued.

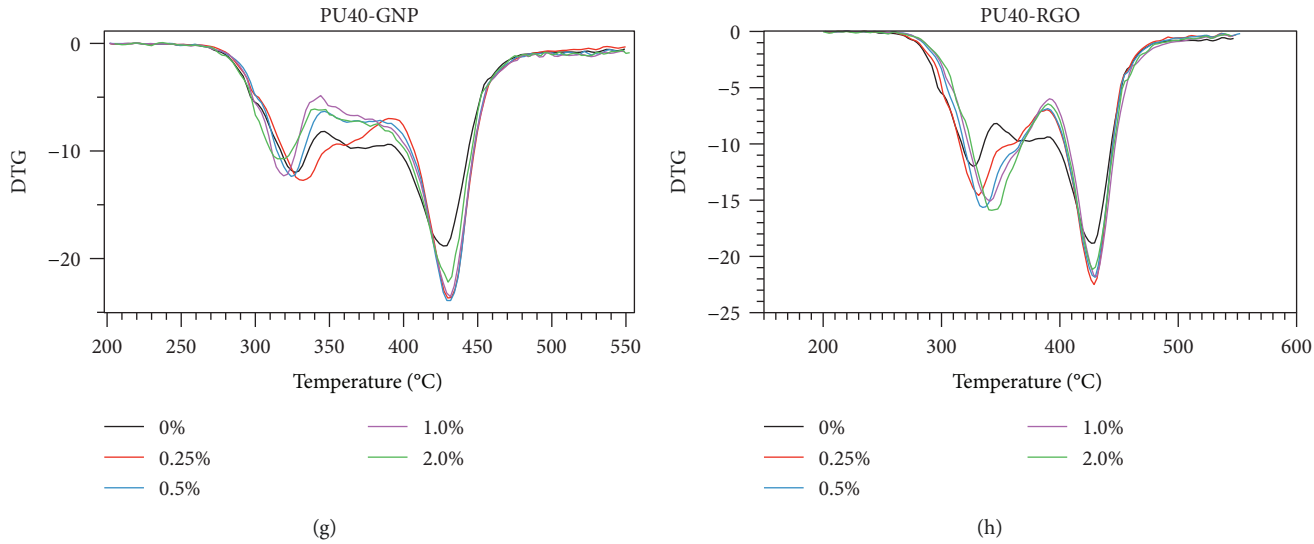

Figure 13: TG curves [%mass versus temperature and derivative (DTG) versus temperature] for PU nanocomposites.

Table 3: TG data for PU nanocomposites.

% nanofiller	PU20-GNP		PU20-RGO		PU40-GNP		PU40-RGO	
	$T_{5\%}$ (°C)	T_{max} (°C)	$T_{5\%}$ (°C)	T_{max} (°C)	$T_{5\%}$ (°C)	T_{max} (°C)	$T_{5\%}$ (°C)	T_{max} (°C)
0.00	295	424	295	424	304	428	304	428
0.25	300	422	302	427	307	431	306	429
0.50	301	422	302	427	307	431	311	429
1.00	299	426	302	431	305	431	312	428
2.00	311	428	303	427	303	431	312	431

$T_{5\%}$: temperature 5% mass loss; T_{max}: temperature of maximum mass loss.

soft segment phase. What is more, at this region the mobility of SS is limited for both amorphous phase and crystalline phase of SS. However, with the temperature increase, the SS crystalline phase melts going completely into the amorphous phase at 20°C.

Addition of the nanofiller causes visible strain changes in comparison to stress behavior, defined as tanδ. For PU20-RGO nanocomposites (Figure 14(f)), values of tanδ are lower with increasing RGO nanofiller content, which is connected with a more elastic behavior of these materials at the investigated temperature range. This is similar for PU20-GNP series (Figure 14(e)), but with the difference that for a 2 wt% addition of GNP there is a rapid increase in tanδ values, which is higher in comparison to the other nanocomposite series and the nonmodified PU matrix. This distinct change probably is related with higher aggregation of the GNP nanofiller, and the increase in loss tangent parameter is the result of the sliding of nanoplatelets, resulting in a decrease in the elasticity of the system, which causes an increase in tanδ values. What is more, the decrease of this parameter for other systems (besides described above) probably is connected with a hydrodynamic effect, where nanofiller particles increase the viscosity of the nanocomposites causing the stiffening of the system.

In the case of PU20-RGO and PU20-GNP nanocomposites, there are noticeable storage modulus (E') changes (Figures 14(a) and 14(b)) in comparison to the PU20 matrix. These E' values are lower up to 1 wt% of the nanofiller content and increase for 2 wt% (RGO of GNP amount), reaching a similar level as for the PU20 matrix. Lower values of the storage modulus (E') (despite increased stiffness) are connected with the weaker adhesion of the nanofiller to the soft segment phase, with movement that is easier on the nanofiller surface.

For polyurethane nanocomposites (PU40-GNP and PU40-RGO), there was a visible (at all investigation temperature range) increase in storage modulus (E') values with the addition of the nanofiller (Figures 15(a) and 15(b)). On the other hand, tanδ changes are different, and for both series this parameter decreases. At up to 0°C for PU40-GNP nanocomposites, a high decrease in tanδ values is observed in comparison to the results for PU40-RGO. This behavior probably means that PU40-GNP possessed higher elasticity. These differences in tanδ values for the two types of the nanocomposite systems evidence a more effective interaction between bordering graphene nanoplatelets (GNP) than in the case of reduced graphene oxide (RGO). It can be expected that the GNP nanofiller creates a more effective network composed of nanofiller particles which are in contact, resulting in a drop of tanδ.

However, it should be highlighted that the stiffness of the nanocomposites, within the discussed temperature range, influences the crystalline phase of the soft domain, which contributes to the stiffening of the pure PU matrix, acting as the physical cross-link of the network. The addition of nanofillers can cause changes in the crystalline structure of these areas, which affect the thermomechanical properties. The fragmentation of the crystalline structure of the soft domain (SS) and the lowering of the crystallinity of these systems may cause an additional decrease in the stiffness of the nanocomposites.

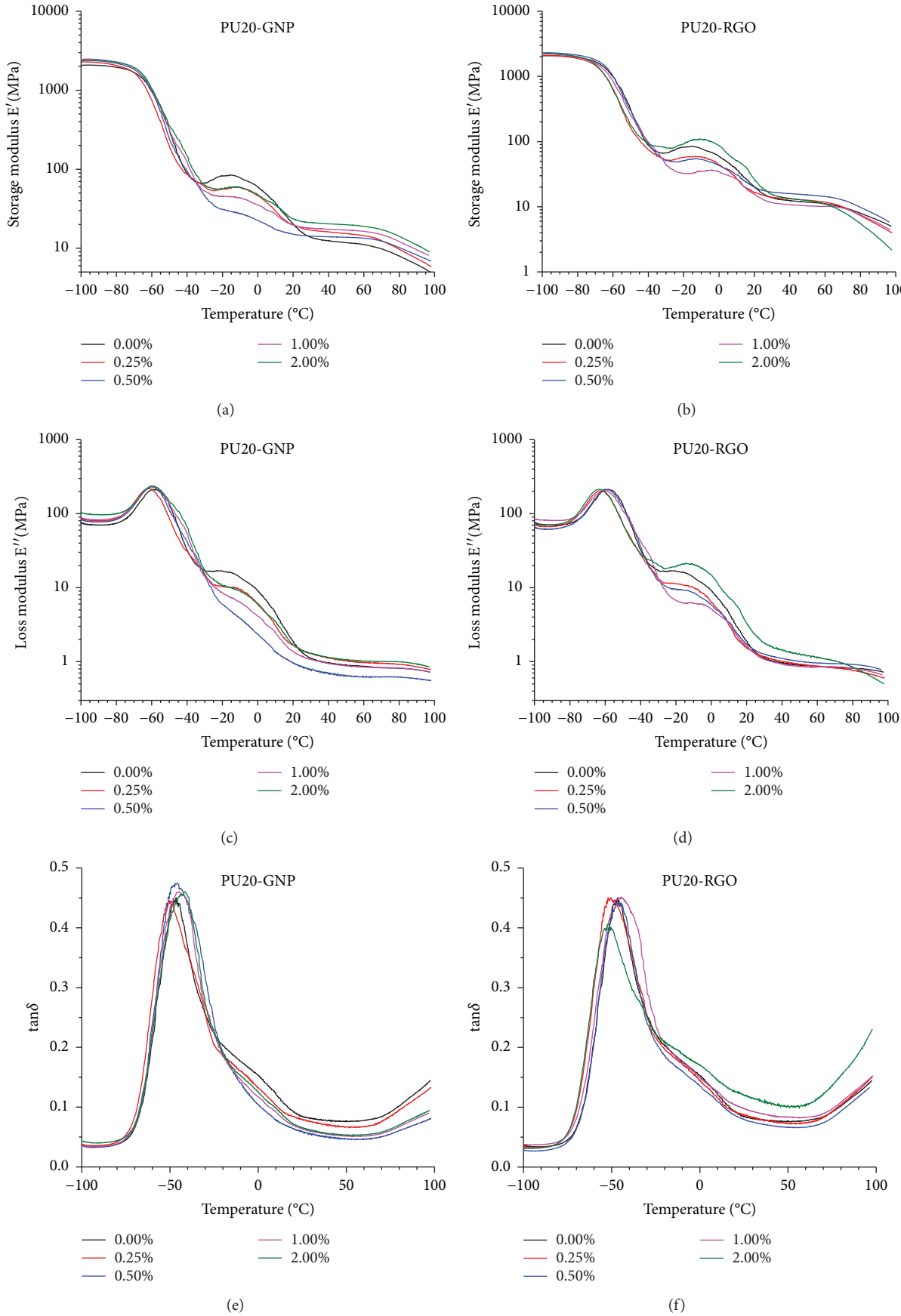

Figure 14: Thermomechanical behavior of PU nanocomposites PU20-GNP and PU20-RGO.

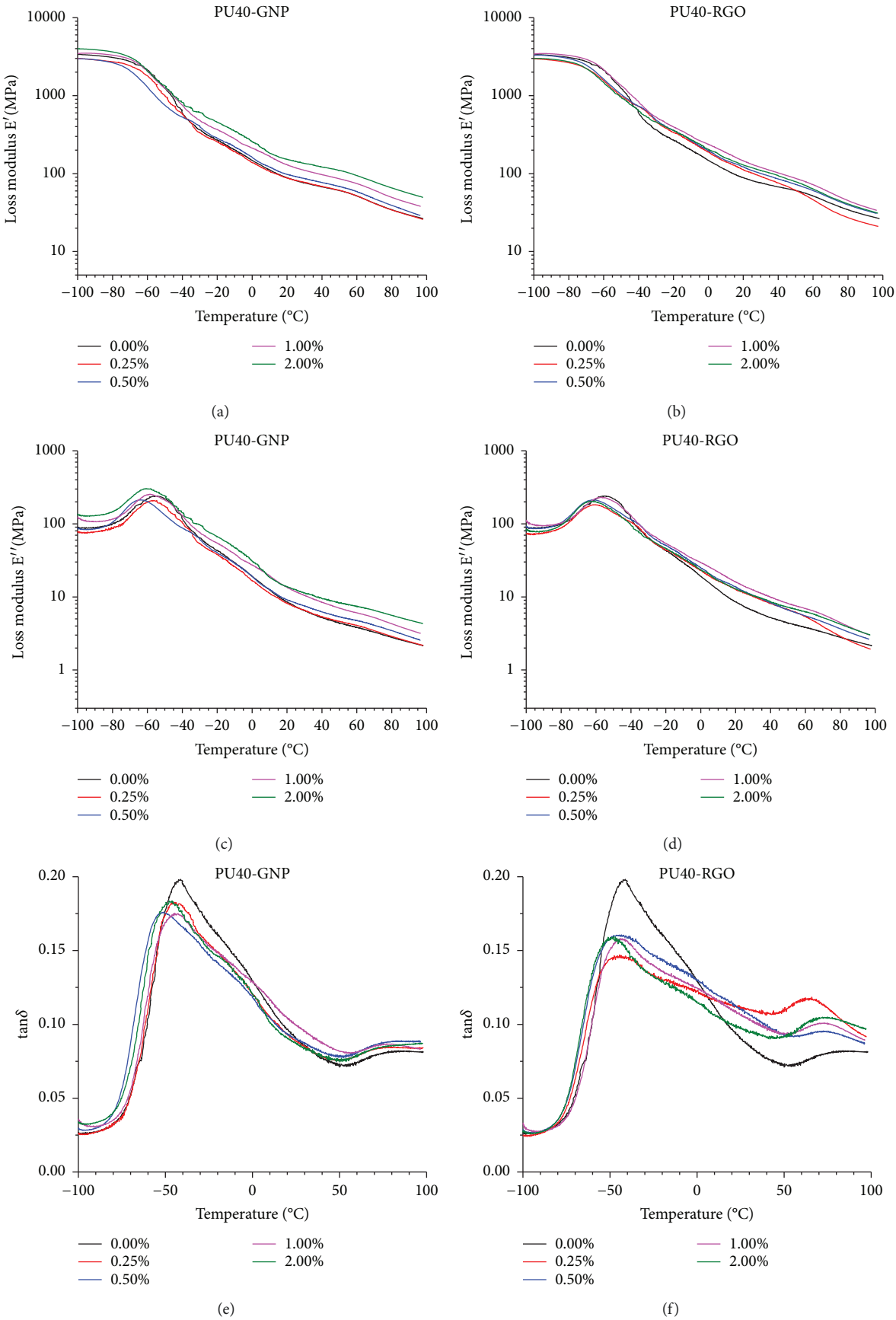

Figure 15: Thermomechanical behavior of PU nanocomposites PU40-GNP and PU40-RGO.

Table 4: Glass transition temperatures for PU and nanocomposite materials.

Materials	Glass transition temperature*/T_g (°C)				
Nanofiller (%)	0	0.25	0.5	1	2
PU20	−46	—	—	—	—
PU40	−42	—	—	—	—
PU20-GNP	—	−50	−46	−45	−42
PU40-GNP	—	−45	−51	−44	−46
PU20-RGO	—	−51	−46	−45	−52
PU40-RGO	—	−45	−45	−43	−48

*Calculated from maximum of loss tangent (tanδ).

(iii) Elastic area (temperature range: 20°C to 100°C)

At this elastic area, all crystallite structures represented by soft segments (SS) are in the amorphous state, above melting temperature. Soft segments have high a degree of free movement, which is limited only by the physical cross-linking network of the hard domain (HS). For all obtained nanocomposite systems, there was a confirmed increase in storage modulus (E') at the elastic plateau region (normal use of PU elastomers) with increasing concentration of the nanofiller. PU20-RGO nanocomposites exhibit a drop at tanδ for the nanofiller content up to 1 wt%, which is connected with a more stiffer behavior of these systems. Further addition of the nanofiller up to 2 wt% results in higher values of tanδ (Figure 14(f)) with a simultaneous increase in loss modulus (E'') (Figure 14(d)), which is the result of the sliding motion of the RGO resulting in the increase of the viscoelasticity. The decrease in tanδ values for the PU20-GNP series was also observed (Figure 14(e)). Likewise, in this case for 2 wt% GNP contents in the polyurethane matrix, there was a noticeable E'' increase, related with a sliding motion (Figure 14(c)). For PU40-RGO and PU40-GNP nanocomposites, the presence of the nanofiller causes an increase in storage modulus (E') values (Figures 15(a) and 15(b)) contributing to the mechanical strength of the nanocomposite. Some differences were also visible for tanδ curves (Figures 15(e) and 15(f)). For PU40-GNP nanocomposites, the shape of the tanδ curve for temperatures above 50°C is similar to the shape of the curve obtained for nonmodified PU (Figure 15(e)). These values also increase with a simultaneous increase in loss modulus (E''), which is correlated with a sliding motion of the GNP nanofiller (in contact with each other) and it causes an increase in E'' (Figure 15(c)). PU40-RGO nanocomposites exhibit an interesting behavior of the tanδ curves, where a maximum of loss tangent appears, connected with a relaxation transformation of melting behavior of the hard domains, which in this case melt at the lower temperature. This is correlated with a lower size of the crystallites, causing a shift of the melting temperature towards lower values. What is more, in comparison to the PU20 nanocomposites, for stiffer matrix (PU40), loss modulus (E'') values increase independently, regardless the amount of the nanofiller (Figure 15(c)).

(2) DMA (Nonlinear Viscoelastic Investigation). A nonlinear viscoelastic behavior of nanocomposite materials was investigated using dynamic mechanical analysis (DMA). All measured series possess three characteristic nonlinear regions (low-amplitude, transition, and high-amplitude). These regions were revealed for all pure polyurethane matrices PU20 and PU40 (Figures 16 and 17). Reinforcement of storage modulus (ΔE/MPa) was calculated as a difference between modulus values at $E_{0.1\%}{}'$ and $E_{10\%}{}'$. All curves (storage modulus versus strain for PU20 matrix) are presented in Figures 16(a) and 16(b).

For polyurethane nanocomposite PU20 containing a minimum 2 wt% GNP nanofiller, a reinforcement effect is observed (higher values of E'). In turn, for RGO nanocomposites, all E' values are similar in comparison to the pure polyurethane matrix (Figures 16(a) and 16(b)). In Figure 17, the difference between modulus change (ΔE) and the increasing amount of nanofiller content into the polyurethane matrix is presented.

A higher effect of the nanofiller content was observed for a harder polyurethane matrix (PU40) in comparison to the softer one (PU20) (Figures 18(a) and 18(b)). Both GNP and RGO nanofillers influence the PU40 matrix which is visible as higher storage modulus (E') values. For PU40 nanocomposites, storage modulus changes (ΔE) are most visible even at low contents of both nanofillers (Figure 19). A sudden drop of E' modulus at the transitional area was not observed, which is characteristic during breakdown of the nanofiller network. What is more, GNP shows a higher interaction with a harder polyurethane matrix (PU40), and a nonlinear viscoelastic behavior is visible for this type of nanofiller.

5. Discussion

The performed investigations of polyurethane nanocomposites, with different hard segment (HS) contents and modified with two types of graphene derivatives (RGO and GNP), revealed the explicit influence of applied nanofillers on morphological, thermal, and mechanical parameters on these systems.

The nanofillers (GNP and RGO) possess a nonpolar character; however, the PU matrix incorporates polar hard segments and the adhesion between these nanofillers and the polyurethane matrix is low. This restricted compatibility of both components (matrix and nanofiller) could be responsible for bigger particle aggregation or agglomeration (100–300 nm length) within the polyurethane matrix, especially for the GNP nanofiller (Figures 10(a) and 10(d)). FTIR investigation did not deliver any clues for the effective interaction between nanofiller (GNP) and matrix (PU) since not even a slight shifting in the position of characteristic bands was observed. There was some agglomeration of the nanofiller with its increasing amount. Based on XRD analysis, some diffraction maxima (representative for GNP nanoplatelets) are visible (Figures 9(a) and 9(c); $2\theta = 27^\circ$), which are connected with multilayer structures, especially for higher content of the GNP (PU40-GNP and PU20-GNP samples). On the other hand, for nanocomposites PU40-RGO and PU20-RGO, there were not visible diffraction maxima (Figures 9(b) and 9(d)), which shows good dispersion and

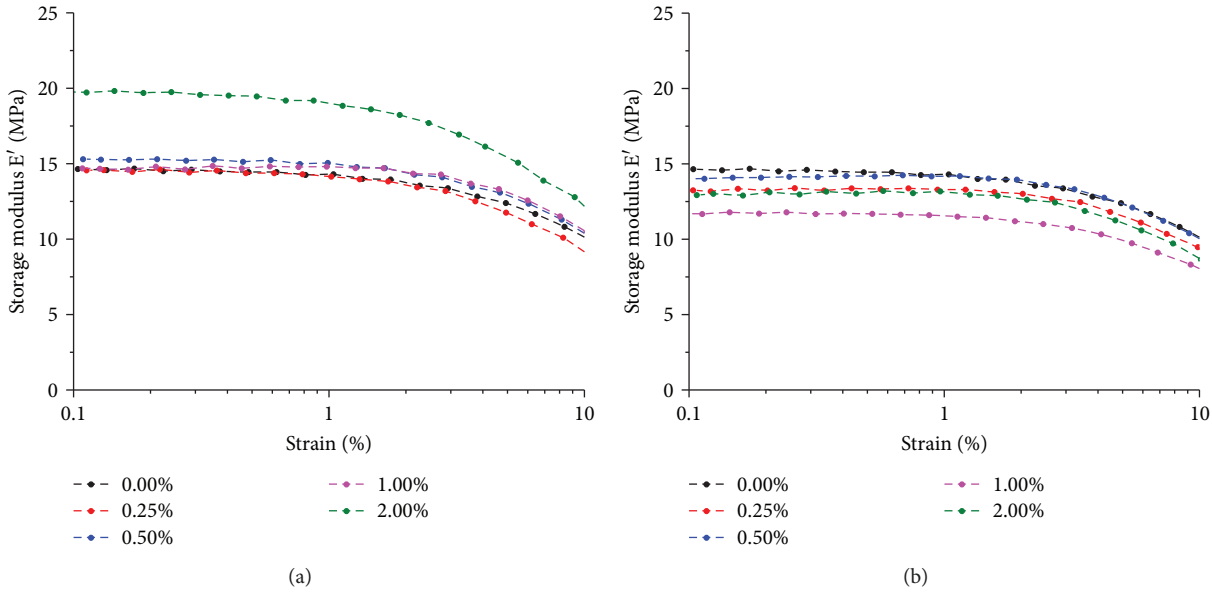

Figure 16: Storage modulus (E'/MPa) versus strain (%) for nanocomposites (a) PU20-GNP and (b) PU20-RGO.

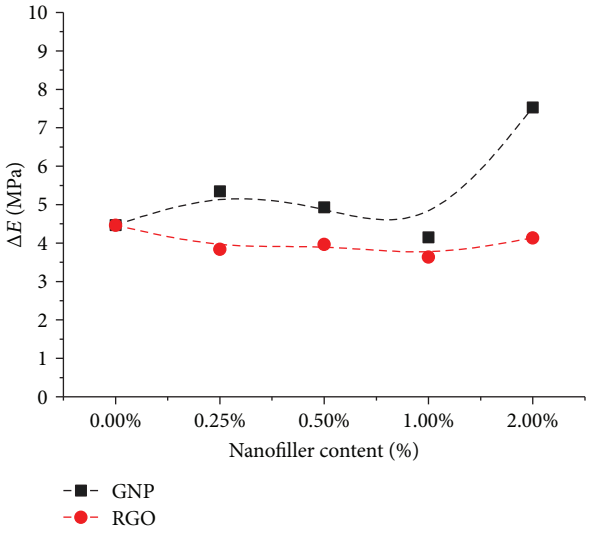

Figure 17: Payne effect improvement ΔE for PU20 nanocomposites.

better compatibility of this type of nanofiller. This result was confirmed using TEM analysis (Figures 10(b), 10(c), 10(e), and 10(f)), where good dispersion of the nanofiller in the polyurethane matrix was achieved. For all obtained nanocomposites (especially for GNP-based systems), it was observed that some part of the nanofiller is highly dispersed into the PU matrix and with higher concentrations of the nanofiller, more agglomerated structures were formed.

Dynamic mechanical analysis allows verifying changes of the basic viscoelastic parameters as a function of temperature for polyurethane nanocomposites with different amounts and different kinds of nanofiller (GNP, RGO). DMA analysis shows that GNP and RGO do not have the same compatibility with the polyurethane matrix. These nanofillers affect both areas of soft and hard segments, where dimensions are similar to the nanofiller surface, but in the glassy state segmental movements of the PU chains disappear and the addition of the nanofiller does not cause significant incensement of storage modulus (E').

Above the glass transition temperature (T_g), a relaxation of soft segments allowing free movement of the nanofiller within the liquid elastic phase was observed. Depending on the kind and amount of the nanofiller, a different effect on the polyurethane matrix was observed. At low nanofiller content (0.5–1.0 wt%), there was a visible increase in the stiffness, connected with the hydrodynamic effect, where stiff nanofiller particles cause higher viscosity of the "liquid" soft domain and that results in higher E' values (Figures 14(a), 14(b) and 15(a) and 15(b)). For higher content of the nanofiller (1.0–2.0 wt%), a further increase in storage modulus (E') and also higher values of the loss modulus (E'') were registered (Figures 14(c), 14(d) and 15(c) and 15(d)). This behavior is the result of a sliding motion of the nanoplatelets (at high nanofiller content) which can be submitted to aggregation and agglomeration. These nanoparticles can clash with one another, causing an increase in mechanical friction, which results in energy dissipation as a result of mechanical loss (increase of loss modulus, E'').

The Payne effect is not visible for all obtained nanocomposite systems. The big role of creating nanofiller network improvement plays as a type of the nanofiller and hard segment content of the polyurethane matrix. For PU20-RGO nanocomposites, the addition of the nanofiller did not change visibly the storage modulus (E'), which is probably connected with the absence of aggregation enlargement after exceeding the threshold of percolation, which allows for effective interactions between the platelets. Comparing PU20-RGO and PU20-GNP samples with 2 wt% nanofiller addition, it was observed that the percolation threshold for

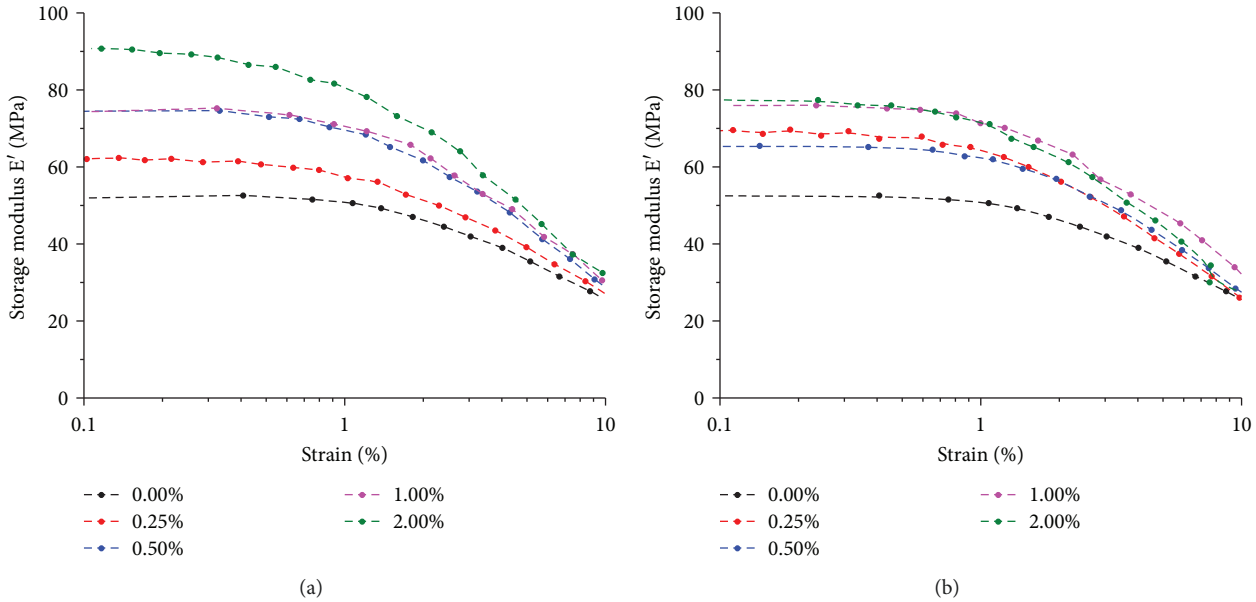

Figure 18: Storage modulus (E'/MPa) versus strain (%) for nanocomposites (a) PU40-GNP and (b) PU40-RGO.

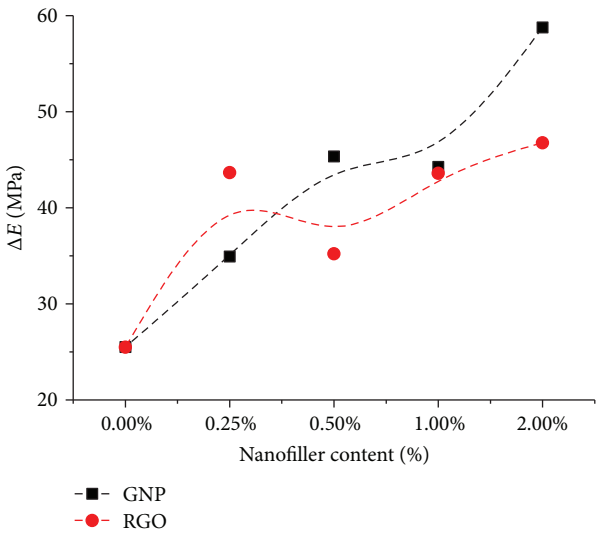

Figure 19: Payne effect improvement ΔE for PU40 nanocomposites.

RGO is higher than for the GNP nanofiller into the PU20 matrix. In PU40 samples, an increase in hard segment (HS) content causes a lower percolation threshold for both nanofillers, where an increase in E' is visible. Addition of these nanofiller leads to an instant increase in E'. The graphene nanoplatelet nanofiller was a more effective modificator, for the PU40 matrix, resulting in a higher E' than the RGO additive.

The hard domain behavior and crystallization process of polyurethane strongly depend on the type of introduced nanofiller and on hard segment (HS) content. Addition of the nanofillers impacts on the crystallization rate, degree of crystallization, and size of the crystallites formed. Table 5 shows the effect of the nanofiller additive on the following: crystallization rate—based on cooling thermograms, resulting from changes in the temperature at which they start to crystallize; effect on crystallinity—decrease in crystallinity was found by the lower values of the melting enthalpy; and influence on the size of forming crystallites—presented on the basis of shifting of melting temperatures (T_m).

Based on observed investigations for nanocomposite systems (PU20-RGO, PU20-GNP, and PU40-RGO), a decrease in crystallinity within the hard domain (Table 5) was conformed. This points to disruption of the hard domain crystallization process caused by the nanofiller, which acts as a physical barrier, reducing the tendency to crystallization. For PU40-GNP polyurethane nanocomposites, a significant influence on the crystallization degree within hard and soft domains was not conformed, but the rate of crystallization in both cases increased. For these samples, creation of hard domain crystallites, which can have larger sizes, was confirmed, which is connected with a shift to higher temperatures of melting temperature peaks with simultaneous disappearance of the preheating area. From the described changes in the crystalline structure of hard domain PU40 nanocomposites, it can be presumed that the crystallization process within these domains is different. Presented differences within HS can be explained by changes in the crystallization process, which depends on the type of nanofiller and also hard segment content in the polyurethane matrices.

For nanocomposites described above, a hard domain melting point is influenced by the fact that all segments (soft and hard) are mixed, while the nanofiller is dispersed between them. At cooling from the melt, the occurring phase separation becomes better with increasing concentration of hard segments. During crystallization of HS, nanoplatelets probably migrate into the soft domain. This behavior can be confirmed by no changes in HS crystallization parameters for PU40-GNP nanocomposites compared to the PU-40

Table 5: Enthalpy of crystallization for PU nanocomposites (cooling scans).

% nanofiller	Cooling scans							
	PU20-GNP		PU20-RGO		PU40-GNP		PU40-RGO	
	$\Delta H_{c,HD}$ (J/g)	$\Delta H_{c,SD}$ (J/g)	$\Delta H_{c,HD}$ (J/g)	$\Delta H_{c,SD}$ (J/g)	$\Delta H_{c,HD}$ (J/g)	$\Delta H_{c,SD}$ (J/g)	$\Delta H_{c,HD}$ (J/g)	$\Delta H_{c,SD}$ (J/g)
0.00	−7.5	—	−7.5	—	−10.3	0.0	−10.3	—
0.25	−5.9	—	−9.0	—	−8.1	−6.5	−8.0	—
0.50	−2.8	—	−4.6	—	−6.3	−6.3	−7.9	—
1.00	−1.6	—	−4.2	—	−5.2	−3.6	−5.2	—
2.00	−2.9	—	−3.3	−4.6	−11.7	−6.3	−12.5	—

Table 6: Comparison of the nanofiller's influence on PU hard and soft domains' behavior.

Samples	Hard domain			Soft domain	
	Crystallization rate	Degree of crystallinity	Crystallite size	Crystallization rate	Degree of crystallinity
PU20-RGO	↑	↓	↓	↑	↓
PU20-GNP	↓	↓	↓	—	↓
PU40-RGO	↓	↓	↓	<–>	↓
PU40-GNP	↑	<–>	↑	↑	<–>

Designation: (↑) increase parameter, (↓) decrease parameter, (<–>) parameter remains unchanged.

elastomer. Lower crystallization enthalpy values for PU40-RGO can be connected with a higher content of RGO, which remains in HS domains causing a decrease in crystallinity and higher crystallite fragmentation. RGO's less tendency to migrate to a soft segment domain (SS) can be due to its folding, smaller flake thickness, and higher polydispersity of its surface area. Also, polar groups on the RGO surface increase the affinity to the rigid segments of PU.

The nanoplatelets migrating into the hard segment domains can accumulate within these structures, and their impact can be enhanced by the hydrodynamic effect and by the creation of the Payne effect but only at a fitting amount of this nanofiller. In the case of nanocomposites PU20-GNP and PU20-RGO, a decrease in crystallinity was observed, indicating that nanoparticles are dispersed in HS domains. As explained above, the migration of RGO is more difficult due to its defected surface structure. The migration of nanofiller particles into hard segment domains for PU20-RGO and PU20-GNP can be less intense or may not occur, because of the small size of the crystalline domains forming from hard segments, which could be connected with a lower amount of HS in these matrices.

Based on the previous investigation, the influence of the nanofillers on phase separation was shown. It can be assumed that the used nanofillers do not have significant influence on the degree of phase separation, with parameter changes fluctuating around 3%. The increasing content of RGO and GNP in the PU20 matrix results in a decrease in the degree of phase separation. What is more, the addition of these nanofillers to the PU40 matrix results in the opposite effect and the increase in the degree of phase separation. The character of these changes correlates with the influence of the nanofillers on the crystallization behavior of HS. For PU20 nanocomposites, a decrease in crystallinity was observed, whereas for PU40 an increasing effect was found only for the GNP nanofiller, not for PU40-RGO samples. With a lower HS content in the PU20 matrix, nanoparticle segregation is smaller, causing more nanoparticles to be present in the hard segment domain thus reducing hydrogen bonding within these crystalline structures. A reverse effect is found for PU40 nanocomposites, where phase separation is higher causing more well-structured hard domains. However, this situation does not coincide for nanocomposites PU20-RGO and PU40-RGO, where phase separation is higher than for PU40-GNP and PU40-RGO. This could be the reason for the heterogeneity of the nanocomposites confirmed by FTIR investigation and of some agglomeration of the nanofiller on the surface of the samples.

6. Conclusions

A clear influence of the nanofillers on the structure, morphology, and thermal and mechanical behavior of the polyurethane nanocomposites was found for two polyurethane matrices possessing different hard segment contents (20% and 40% HS) modified with graphene derivatives (reduced graphene oxide (RGO) and graphene nanoplatelets (GNP)) (Table 6). Differences in the properties of the obtained nanocomposites result mainly from the change in the morphological structure of these nanocomposites as a result of the introduction of nanofillers. Obtaining nanocomposites with a different content of the nanofiller allowed following the changes in the structure and properties of nanocomposites. The addition of both types of graphene forms influenced the crystalline structure of hard and soft domains. The use of the polyurethane matrix with a different content of rigid segments revealed a different way in which crystallization and melting processes occur within both domains present. It has been found, depending on the filled matrix, that the graphene form may cause a decrease in the degree of

crystallinity and delay the crystallization process or may exhibit a nucleating behavior.

Based on changes in crystallinity, the crystallization process occurring in the presence of nanofillers in polyurethane matrices was examined. A properly selected type of graphene nanofiller and its appropriate amount allows improving the elastic properties of polyurethane materials, as a result of hydrodynamic reinforcement connected with the creation of Payne's reinforcing aggregation network.

Data Availability

The data used to support the findings of this study are available from the corresponding author upon request.

Conflicts of Interest

The author declares that there is no conflict of interest regarding the publication of this paper.

Acknowledgments

The author acknowledges Piotr Korzeniewski (Poland), who prepared the PU nanocomposite samples, and Anu A. S. (India) for performing TEM experiments. Special acknowledgments are due to Professor Sabu Thomas (India) for his support.

References

[1] M. Bhattacharya, "Polymer nanocomposites—a comparison between carbon nanotubes, graphene, and clay as nanofillers," *Materials*, vol. 9, no. 4, p. 262, 2016.

[2] M. Šupová, G. S. Martynková, and K. Barabaszová, "Effect of nanofillers dispersion in polymer matrices: a review," *Science of Advanced Materials*, vol. 3, no. 1, pp. 1–25, 2011.

[3] M. Damien, E. S. Guillaume, and C. Chivas-Joly, "Properties of nanofillers in polymer," in *Nanocomposites and Polymers with Analytical Methods*, 2011.

[4] H. Kim, S. Kobayashi, M. A. AbdurRahim et al., "Graphene/polyethylene nanocomposites: effect of polyethylene functionalization and blending methods," *Polymer*, vol. 52, no. 8, pp. 1837–1846, 2011.

[5] M. Z. Iqbal, A. A. Abdala, V. Mittal, S. Seifert, A. M. Herring, and M. W. Liberatore, "Processable conductive graphene/polyethylene nanocomposites: effects of graphene dispersion and polyethylene blending with oxidized polyethylene on rheology and microstructure," *Polymer*, vol. 98, pp. 143–155, 2016.

[6] S. Park, S. He, J. Wang, A. Stein, and C. W. Macosko, "Graphene-polyethylene nanocomposites: effect of graphene functionalization," *Polymer*, vol. 104, pp. 1–9, 2016.

[7] X. Fu, C. Yao, and G. Yang, "Recent advances in graphene/polyamide 6 composites: a review," *RSC Advances*, vol. 5, no. 76, pp. 61688–61702, 2015.

[8] X. Liu, X. Y. Shao, G. B. Fang, H. F. He, and Z. G. Wan, "Preparation and properties of chemically reduced graphene oxide/copolymer-polyamide nanocomposites," *E-Polymers*, vol. 17, no. 1, pp. 3–14, 2017.

[9] A. O'Neill, D. Bakirtzis, and D. Dixon, "Polyamide 6/graphene composites: the effect of in situ polymerisation on the structure and properties of graphene oxide and reduced graphene oxide," *European Polymer Journal*, vol. 59, pp. 353–362, 2014.

[10] T. Kuila, S. Bose, P. Khanra, N. H. Kim, K. Y. Rhee, and J. H. Lee, "Characterization and properties of in situ emulsion polymerized poly(methyl methacrylate)/graphene nanocomposites," *Composites Part A: Applied Science and Manufacturing*, vol. 42, no. 11, pp. 1856–1861, 2011.

[11] S. Morimune, T. Nishino, and T. Goto, "Ecological approach to graphene oxide reinforced poly (methyl methacrylate) nanocomposites," *ACS Applied Materials & Interfaces*, vol. 4, no. 7, pp. 3596–3601, 2012.

[12] R. Shah, A. Kausar, and B. Muhammad, "Characterization and properties of poly(methyl methacrylate)/graphene, poly(methyl methacrylate)/graphene oxide and poly(methyl methacrylate)/*p*-phenylenediamine-graphene oxide nanocomposites," *Polymer-Plastics Technology and Engineering*, vol. 54, no. 13, pp. 1334–1342, 2015.

[13] H. Hu, X. Wang, J. Wang et al., "Preparation and properties of graphene nanosheets-polystyrene nanocomposites via in situ emulsion polymerization," *Chemical Physics Letters*, vol. 484, no. 4-6, pp. 247–253, 2010.

[14] A. S. Patole, S. P. Patole, S. Y. Jung, J. B. Yoo, J. H. An, and T. H. Kim, "Self assembled graphene/carbon nanotube/polystyrene hybrid nanocomposite by in situ microemulsion polymerization," *European Polymer Journal*, vol. 48, no. 2, pp. 252–259, 2012.

[15] Z. He, B. Zhang, H. B. Zhang et al., "Improved rheological and electrical properties of graphene/polystyrene nanocomposites modified with styrene maleic anhydride copolymer," *Composites Science and Technology*, vol. 102, pp. 176–182, 2014.

[16] M. Hernández, M. . M. Bernal, R. Verdejo, T. A. Ezquerra, and M. A. López-Manchado, "Overall performance of natural rubber/graphene nanocomposites," *Composites Science and Technology*, vol. 73, pp. 40–46, 2012.

[17] A. Malas, "Rubber nanocomposites with graphene as the nanofiller," in *Progress in Rubber Nanocomposites*, pp. 179–229, Woodhead Publishing Series in Composites Science and Engineering, 2017.

[18] K. K. Sadasivuni, D. Ponnamma, J. Kim, and S. Thomas, *Graphene-Based Polymer Nanocomposites in Electronics*, Springer Series on Polymer and Composite Materials, Springer International Publishing, 2015.

[19] S. Thomas and R. Stephen, *Rubber Nanocomposites: Preparation, Properties, and Applications*, Wiley, 2010.

[20] H. Kim, Y. Miura, and C. W. MacOsko, "Graphene/polyurethane nanocomposites for improved gas barrier and electrical conductivity," *Chemistry of Materials*, vol. 22, no. 11, pp. 3441–3450, 2010.

[21] S. K. Yadav and J. W. Cho, "Functionalized graphene nanoplatelets for enhanced mechanical and thermal properties of polyurethane nanocomposites," *Applied Surface Science*, vol. 266, pp. 360–367, 2013.

[22] M. Kumar, J. S. Chung, B. S. Kong, E. J. Kim, and S. H. Hur, "Synthesis of graphene-polyurethane nanocomposite using highly functionalized graphene oxide as pseudo-crosslinker," *Materials Letters*, vol. 106, pp. 319–321, 2013.

[23] M. Verma, S. S. Chauhan, S. K. Dhawan, and V. Choudhary, "Graphene nanoplatelets/carbon nanotubes/polyurethane composites as efficient shield against electromagnetic polluting radiations," *Composites Part B: Engineering*, vol. 120, pp. 118–127, 2017.

[24] Y. R. Lee, A. V. Raghu, H. M. Jeong, and B. K. Kim, "Properties of waterborne polyurethane/functionalized graphene sheet nanocomposites prepared by an in situ method," *Macromolecular Chemistry and Physics*, vol. 210, no. 15, pp. 1247–1254, 2009.

[25] M. N. Muralidharan and S. Ansari, "Thermally reduced graphene oxide/thermoplastic polyurethane nanocomposites as photomechanical actuators," *Advanced Materials Letters*, vol. 4, no. 12, pp. 927–932, 2013.

[26] D. K. Pradhan, R. N. P. Choudhary, and B. K. Samantaray, "Studies of dielectric and electrical properties of plasticized polymer nanocomposite electrolytes," *Materials Chemistry and Physics*, vol. 115, no. 2-3, pp. 557–561, 2009.

[27] Y. Li, D. Pan, S. Chen, Q. Wang, G. Pan, and T. Wang, "In situ polymerization and mechanical, thermal properties of polyurethane/graphene oxide/epoxy nanocomposites," *Materials and Design*, vol. 47, pp. 850–856, 2013.

[28] P. Pokharel, S. Choi, and D. S. Lee, "The effect of hard segment length on the thermal and mechanical properties of polyurethane/graphene oxide nanocomposites," *Composites Part A: Applied Science and Manufacturing*, vol. 69, pp. 168–177, 2015.

[29] X. Qian, L. Song, Q. Tai, Y. Hu, and R. K. K. Yuen, "Graphite oxide/polyurea and graphene/polyurea nanocomposites: a comparative investigation on properties reinforcements and mechanism," *Composites Science and Technology*, vol. 74, pp. 228–234, 2013.

[30] I. S. Fahim, "A nanoscale investigation of mechanical, thermal stability and electrical conductivity properties of reinforced thermoplastic polyurethane/graphene nanocomposite," *American Journal of Nanoscience and Nanotechnology*, vol. 1, no. 1, pp. 31–40, 2013.

[31] M. A. Hood, B. Wang, J. M. Sands, J. J. la Scala, F. L. Beyer, and C. Y. Li, "Morphology control of segmented polyurethanes by crystallization of hard and soft segments," *Polymer*, vol. 51, no. 10, pp. 2191–2198, 2010.

[32] M. C. Lopes, H. Ribeiro, M. C. Gonçalves Santos et al., "High performance polyurethane composites with isocyanate-functionalized carbon nanotubes: improvements in tear strength and scratch hardness," *Journal of Applied Polymer Science*, vol. 134, no. 2, article 44394, 2017.

[33] S. Rana, J. W. Cho, and L. P. Tan, "Graphene-crosslinked polyurethane block copolymer nanocomposites with enhanced mechanical, electrical, and shape memory properties," *RSC Advances*, vol. 3, no. 33, p. 13796, 2013.

[34] D. A. Nguyen, Y. R. Lee, A. V. Raghu, H. M. Jeong, C. M. Shin, and B. K. Kim, "Morphological and physical properties of a thermoplastic polyurethane reinforced with functionalized graphene sheet," *Polymer International*, vol. 58, no. 4, pp. 412–417, 2009.

[35] D. B. Klinedinst, I. Yilgör, E. Yilgör, M. Zhang, and G. L. Wilkes, "The effect of varying soft and hard segment length on the structure–property relationships of segmented polyurethanes based on a linear symmetric diisocyanate, 1,4-butanediol and PTMO soft segments," *Polymer*, vol. 53, no. 23, pp. 5358–5366, 2012.

[36] I. V. Khudyakov, D. R. Zopf, and N. J. Turro, "Polyurethane nanocomposites," *Designed Monomers and Polymers*, vol. 12, no. 4, pp. 279–290, 2009.

[37] B. Xu, Y. Q. Fu, W. M. Huang et al., "Thermal-mechanical properties of polyurethane-clay shape memory polymer nanocomposites," *Polymers*, vol. 2, no. 2, pp. 31–39, 2010.

[38] A. V. Rane, K. Kanny, V. K. Abitha, S. Jadhav, S. Mulge, and S. Thomas, "Applications of polyurethane based composites and nanocomposites," in *Polyurethane Polymers*, S. Thomas, J. Datta, J. T. Haponiuk, and A. Reghunadhan, Eds., pp. 559–573, Elsevier, Amsterdam, 2017.

[39] P. K. Maji, "Graphene-based polymer nanocomposites: materials for future revolution," *MOJ Polymer Science*, vol. 1, no. 3, pp. 94–97, 2017.

[40] A. Kausar, "Emerging research trends in polyurethane/graphene nanocomposite: a review," *Polymer-Plastics Technology and Engineering*, vol. 56, no. 13, pp. 1468–1486, 2017.

[41] https://www.acsmaterial.com/graphene-nanoplatelets-2-10nm-1204.html.

[42] M. Strankowski, P. Korzeniewski, J. Strankowska, A. S. Anu, and S. Thomas, "Morphology, mechanical and thermal properties of thermoplastic polyurethane containing reduced graphene oxide and graphene nanoplatelets," *Materials*, vol. 11, no. 1, p. 82, 2018.

[43] D. C. Marcano, D. V. Kosynkin, J. M. Berlin et al., "Improved synthesis of graphene oxide," *ACS Nano*, vol. 4, no. 8, pp. 4806–4814, 2010.

[44] A. V. Raghu, G. S. Gadaginamath, N. Mathew, S. B. Halligudi, and T. M. Aminabhavi, "Synthesis, characterization, and acoustic properties of new soluble polyurethanes based on 2,2′-[1,4-phenylenebis(nitrilomethylylidene)]diphenol and 2,2′-[4,4′-methylene-di-2-methylphenylene-1,1′-bis(nitrilomethylylidene)]diphenol," *Journal of Applied Polymer Science*, vol. 106, no. 1, pp. 299–308, 2007.

[45] A. V. Raghu, H. M. Jeong, J. H. Kim, Y. R. Lee, Y. B. Cho, and K. Sirsalmath, "Synthesis and characterization of novel polyurethanes based on 4-{(4-hydroxyphenyl)iminomethyl}phenol," *Macromolecular Research*, vol. 16, no. 3, pp. 194–199, 2008.

[46] B. Janowski, K. Pielichowski, and R. Kwiatkowski, "Nanohybrid polyurethane (PUR)/functionalized silsesquioxane (PHIPOSS) systems. Part II. X-Ray structural investigations using WAXD and SAXS methods," *Polimery*, vol. 59, no. 2, pp. 147–159, 2014.

[47] P. K. Maji and A. K. Bhowmick, "Structure-property correlation of polyurethane nanocomposites: influence of loading and nature of nanosilica and microstructure of hyperbranched polyol," *Journal of Applied Polymer Science*, vol. 127, no. 6, pp. 4492–4504, 2013.

[48] D. Ponnamma, K. K. Sadasivuni, M. Strankowski, P. Moldenaers, S. Thomas, and Y. Grohens, "Interrelated shape memory and Payne effect in polyurethane/graphene oxide nanocomposites," *RSC Advances*, vol. 3, no. 36, p. 16068, 2013.

[49] K. Bagdi, K. Molnár, I. Sajó, and B. Pukánszky, "Specific interactions, structure and properties in segmented polyurethane elastomers," *Express Polymer Letters*, vol. 5, no. 5, pp. 417–427, 2011.

[50] J. A. Hiltz and J. P. Szabo, *FT-IR Study of Poly(ether)urethanes*, Def. Res. Est. Atl, 2001.

[51] H. S. Lee, Y. K. Wang, and S. L. Hsu, "Spectroscopic analysis of phase separation behavior of model polyurethanes," *Macromolecules*, vol. 20, no. 9, pp. 2089–2095, 1987.

[52] P. Zhao, Y. S. Wang, J. H. Zhu, X. Y. Hua, and Q. Z. Wen, "Characterization of graded polyurethane elastomer by FTIR," *Science in China Series B: Chemistry*, vol. 51, no. 1, pp. 58–61, 2008.